




Convergent effects of a functional C3 variant on brain atrophy, demyelination, and cognitive impairment in multiple sclerosis

Tina Roostaei, Shokufeh Sadaghiani, Rahil Mashhadi, Masih Falahatian, Esmaeil Mohamadi, Nina Javadian, Aria Nazeri, Rozita Doosti, Abdorreza Naser Moghadasi, Mahsa Owji, Amir Pejman Hashemi Taheri, Ali Shakouri Rad, Amirreza Azimi, Aristotle N Voineskos, Arash Nazeri  and Mohammad Ali Sahraian

Abstract

Background: Complement system activation products are present in areas of neuroinflammation, demyelination, and neurodegeneration in brains of patients with multiple sclerosis (MS). C3 is a central element in the activation of complement cascades. A common coding variant in the C3 gene (rs2230199, C3R102G) affects C3 activity.

Objectives: To assess the effects of rs2230199 on MS severity using clinical, cognitive, and imaging measures.

Methods: In total, 161 relapse-onset MS patients (Expanded Disability Status Scale (EDSS) ≤ 6) underwent physical assessments, cognitive tests (Paced Auditory Serial Addition Test (PASAT), Symbol Digit Modalities Test (SDMT), and California Verbal Learning Test (CVLT)), and magnetic resonance imaging (MRI). Lesion volumes were quantified semi-automatically. Voxel-wise analyses were performed to assess the effects of rs2230199 genotype on gray matter (GM) atrophy ($n = 155$), white matter (WM) fractional anisotropy (FA; $n = 105$), and WM magnetization transfer ratio (MTR; $n = 90$).

Results: While rs2230199 minor-allele dosage (C3-102G) showed no significant effect on EDSS and Multiple Sclerosis Functional Composite (MSFC), it was associated with worse cognitive performance ($p = 0.02$), lower brain parenchymal fraction ($p = 0.003$), and higher lesion burden ($p = 0.02$). Moreover, voxel-wise analyses showed lower GM volume in subcortical structures and insula, and lower FA and MTR in several WM areas with higher copies of rs2230199 minor allele.

Conclusion: C3-rs2230199 affects white and GM damage as well as cognitive impairment in MS patients. Our findings support a causal role for complement system activity in the pathophysiology of MS.

Keywords: Native immunity, complement component 3, diffusion-weighted MRI, magnetization transfer contrast imaging, imaging genetics, diffusion tensor imaging

Date received: 8 February 2017; revised: 17 January 2018; accepted: 31 January 2018

Introduction

Multiple sclerosis (MS) is a complex autoimmune inflammatory disease affecting the central nervous system (CNS). The complement system is a key component of the innate immune system that has been strongly implicated in the pathogenesis of MS.¹ Complement component 3 (C3) is a central element in the activation of both alternative and classical complement cascades. C3 is believed to be involved in the pathogenesis of MS through its role in demyelination, neurodegeneration, and neuroinflammation.

Findings from human postmortem studies support the evidence from in vitro and animal studies on the role of C3 in MS. Autopsy studies have consistently detected C3 cleavage products in the active white matter (WM) lesions, at the edges of chronic active lesions, and on partly demyelinated axons located in normal-appearing peri-plaque WM in MS,²⁻⁶ suggesting involvement of C3 in WM demyelination. Moreover, C3 activation products have been localized at engulfed synapses by microglia within the hippocampus of patients with MS,⁷ suggesting C3's

Correspondence to:
Arash Nazeri
Mallinckrodt Institute of
Radiology, Washington
University School of
Medicine, 510 South
Kingshighway Blvd.,
Campus Box 8131, St. Louis,
MO 63110, USA.
arashnazeri@gmail.com

Mohammad Ali Sahraian
Multiple Sclerosis Research
Center, Neuroscience
Institute, Tehran University
of Medical Sciences and Sina
Hospital, Hassan Abad Sq.,
Tehran 1136746911, Iran.
msahrai@tums.ac.ir

Tina Roostaei
Multiple Sclerosis Research
Center, Neuroscience
Institute, Tehran University
of Medical Sciences and
Sina Hospital, Tehran,
Iran/Interdisciplinary
Neuroscience Research
Program, Tehran University
of Medical Sciences,
Tehran, Iran/Kimel Family
Translational Imaging-
Genetics Laboratory,
Research Imaging Centre,
Campbell Family Mental
Health Research Institute,
Centre for Addiction
and Mental Health,
Toronto, ON, Canada/
Department of Psychiatry,
University of Toronto,
Toronto, ON, Canada/
Center for Translational
and Computational
Neuroimmunology,
Department of Neurology,
Columbia University
Medical Center, New York,
NY, USA

Shokufeh Sadaghiani
Multiple Sclerosis Research
Center, Neuroscience
Institute, Tehran University
of Medical Sciences and
Sina Hospital, Tehran, Iran/
Interdisciplinary Neuroscience
Research Program, Tehran
University of Medical
Sciences, Tehran, Iran

Rahil Mashhadi
Urology Research Center,
Tehran University of
Medical Sciences, Tehran,
Iran

Masih Falahatian
Multiple Sclerosis Research
Center, Neuroscience
Institute, Tehran University
of Medical Sciences and
Sina Hospital, Tehran, Iran/
School of Medicine, Isfahan
University of Medical
Sciences, Isfahan, Iran

Esmail Mohamadi
Nina Javadian

Rozita Doosti
Mahsa Owji
Multiple Sclerosis Research
Center, Neuroscience
Institute, Tehran University
of Medical Sciences and
Sina Hospital, Tehran, Iran

Aria Nazeri
Multiple Sclerosis Research
Center, Neuroscience
Institute, Tehran University
of Medical Sciences and
Sina Hospital, Tehran, Iran/
Mallinckrodt Institute of
Radiology, Washington
University School of
Medicine, St. Louis, MO,
USA

Abdorrezza Naser
Moghadasi
Amirreza Azimi
Mohammad Ali Sahraian
Multiple Sclerosis Research
Center, Neuroscience
Institute, Tehran University
of Medical Sciences and
Sina Hospital, Tehran,
Iran/Iranian Center of
Neurological Research,
Neuroscience Institute,
Tehran University of
Medical Sciences, Tehran,
Iran

Amir Pejman Hashemi
Taheri
Ali Shakouri Rad
Department of Radiology,
Tehran University of
Medical Sciences, Tehran,
Iran

Aristotle N Voineskos
Kimel Family Translational
Imaging-Genetics
Laboratory, Research
Imaging Centre, Campbell
Family Mental Health
Research Institute, Centre
for Addiction and Mental
Health, Toronto, ON,
Canada/Department of
Psychiatry, University of
Toronto, Toronto, ON,
Canada

Arash Nazeri
Multiple Sclerosis Research
Center, Neuroscience
Institute, Tehran University
of Medical Sciences and
Sina Hospital, Tehran,
Iran/Interdisciplinary
Neuroscience Research
Program, Tehran University
of Medical Sciences,

contribution to synapse elimination and gray matter (GM) atrophy. Finally, C3 fragments have been detected along myelinated nerve fibers in close proximity of primed microglia in normal-appearing WM of MS patients,⁸ supporting C3's role in microglial priming and the resulting neuroinflammation (i.e. multiplication and activation of microglia, which can trigger an exaggerated response to a secondary inflammatory stimulus⁹).

A common coding variant in the C3 gene (C3R102G (arginine to glycine) or rs2230199 G → C; minor allele frequency ~0.2 in European populations) is an established genetic risk factor for age-related macular degeneration.¹⁰ Compared with C3-102R (rs2230199^G, major allele), C3-102G (rs2230199^C, minor allele) has lower affinity for factor H (the master regulator of complement activation) which results in enhanced alternative pathway amplification.¹¹ In addition, C3-102G has a higher capacity to bind onto mononuclear cells than C3-102R¹² that is relevant to both classical and alternative complement pathways.

The findings from postmortem human studies associating C3 with MS pathophysiology do not necessarily provide a causal link between complement system activity and demyelination, neurodegeneration, and neuroinflammation in MS. Moreover, findings from in vitro and animal studies are not necessarily generalizable to human. Here, utilizing a genetic association approach, we aimed to assess whether there is evidence supporting a causal role for C3 in the pathogenesis of MS in human. We hypothesized that C3-102G allele would have detrimental effects on GM atrophy and WM demyelination measures and ultimately clinical severity and cognitive impairment in MS. In addition to global brain atrophy and lesion load, we assessed the effects of C3R102G on regional GM atrophy (using T₁-weighted magnetic resonance imaging (MRI)), integrity of WM tracts (using diffusion-weighted MRI), and regional WM demyelination (using magnetization transfer imaging).¹³

Methods

Participants

Data were obtained from the Cross-modal Research Initiative for Multiple Sclerosis and Optic Neuritis (CRIMSON) observational study,¹⁴ in which clinical, cognitive, neuroimaging, and genetic data were collected with the aim to identify the determinants of MS severity and progression. Individuals with relapse-onset MS (based on the 2010 McDonald criteria) were enrolled (2012–2014) based on referrals from

the Multiple Sclerosis Research Center, Tehran, Iran, and the MS Society of Iran (age: 18–59 years; Expanded Disability Status Scale¹⁵ (EDSS) ≤ 6). The study was approved by the Ethics Review Board of Tehran University of Medical Sciences. All participants provided written informed consent, underwent clinical and cognitive evaluation and brain MRI, and donated blood for genetic studies.

Exclusion criteria included the following: history of clinical relapse or corticosteroid therapy in the last 12 weeks prior to enrollment, self-reported history of neurological disorders (other than MS), psychotic disorders, head trauma with loss of consciousness, and cancer, in addition to concurrent chronic systemic medical illness, uncontrolled thyroid dysfunction, and substance abuse.

Clinical and cognitive evaluation

MS clinical severity was assessed using EDSS and Multiple Sclerosis Functional Composite (MSFC). Cognitive performance was assessed using¹⁶ Paced Auditory Serial Addition Test (PASAT; part of MSFC), California Verbal Learning Test (CVLT; total learning score), and Symbol Digit Modalities Test¹⁷ (SDMT). A composite cognitive score was calculated for each individual by averaging the z-scores for their performance on the three cognitive tests.

Genotyping

Ethylenediaminetetraacetic acid (EDTA)-anticoagulated whole blood samples were stored at –80°C. DNA extraction was performed using DNeasy Blood & Tissue Kit (Qiagen). rs2230199 was genotyped using polymerase chain reaction (PCR) amplification and subsequent restriction-fragment length polymorphism (RFLP) analysis with *HhaI* restriction endonuclease as described previously.¹⁸

MRI

Brain MRI was carried out at either of the two imaging sites using 1.5-T Siemens scanners (Magnetom Avanto scanner (Shariati Hospital) and Magnetom Symphony (Sina Hospital)).

The imaging protocols at the Shariati Hospital were as follows: (1) sagittal three-dimensional (3D) magnetization-prepared rapid gradient echo (MPRAGE) T₁-weighted images: two repetitions, repetition time (TR) = 2730 ms, echo time (TE) = 2.81 ms, inversion time (TI) = 1000 ms, flip angle = 7°, and voxel dimension = 1 × 1 × 1 mm³; (2) single-shot spin-echo

diffusion-weighted echoplanar images: 64 noncollinear gradient orientations at $b = 1000$ s/mm² along with three $b = 0$ s/mm² volumes, TR = 9500 ms, TE = 93 ms, and voxel dimension = $2 \times 2 \times 2.1$ mm³; (3) 3D T₂-weighted sampling-perfection with application optimized contrasts using different flip angle evolution (SPACE) images: TR = 3200 ms, TE = 473 ms, and voxel dimension = $1 \times 1 \times 1$ mm³; and (4) T₂ fluid-attenuated inversion recovery (FLAIR) turbo spin-echo images: TR = 9400 ms, TE = 83 ms, TI = 2500 ms, and voxel dimension = $1.3 \times 1 \times 3$ mm³.

Images were acquired at the Sina Hospital using the following imaging protocols: (1) sagittal 3D fast low angle shot (FLASH) T₁-weighted: TR = 22 ms, TE = 9.2 ms, flip angle = 30°, and voxel dimension = $1.2 \times 1.2 \times 1.2$ mm³; (2) single-shot spin-echo diffusion-weighted echoplanar images: 2 repetitions, 12 noncollinear gradient orientations at $b = 1000$ s/mm² plus 1 $b = 0$ s/mm² volume, TR = 10,500 ms, TE = 132 ms, and voxel dimension = $1.8 \times 1.8 \times 3$ mm³ (added later to the imaging protocol and available only from a number of participants); (3) magnetization transfer images (gradient echo images once with and once without a magnetization transfer pulse, MT_{ON} and MT_{OFF}, respectively): TR = 35 ms, TE = 11 ms, flip angle = 15°, and voxel dimension = $1 \times 1 \times 3$ mm³; (4) T₂-weighted turbo spin-echo images: TR = 5800 ms, TE = 92 ms, and voxel dimension = $1 \times 1 \times 3$ mm³; and (v) T₂ FLAIR turbo spin-echo images: TR = 9400 ms, TE = 86 ms, TI = 2500 ms, and voxel dimension = $1.3 \times 1 \times 3$ mm³.

Lesion segmentation and T₁-weighted image preprocessing

As two T₁-weighted repetitions were obtained for each individual at the Shariati imaging site, the second image was registered to the first image (using FLIRT, part of FSL v5.0.9, www.fmrib.ox.ac.uk/fsl) and the two images were averaged in order to make a single T₁-weighted image used in further analyses.

T₂-hyperintense lesions were segmented manually by an expert rater (A.N.) according to the MRI atlas of MS lesions,¹⁹ and total brain lesion volumes were calculated for each individual. T₂-weighted images were linearly registered to their corresponding T₁-weighted images, and the resulting registration matrices were used to align the lesion masks with T₁-weighted images. Voxels corresponding to lesions in T₁-weighted images were filled with intensities similar to normal-appearing WM using the Lesion Segmentation Toolbox (<http://www.applied-statistics.de/lst.html>) in order to minimize lesion-induced errors in brain tissue segmentation and template registration.

Brain tissue segmentation and voxel-based morphometry preprocessing

Filled T₁-weighted images were used for brain tissue segmentation and voxel-based morphometry (VBM)²⁰ preprocessing using SPM8 (<http://www.fil.ion.ucl.ac.uk/spm/software/spm8/>) and the VBM8 toolbox (<http://dbm.neuro.uni-jena.de/vbm.html>) with default parameters. Briefly, images were corrected for intensity nonuniformity and segmented into three brain tissue classes (GM, WM, and cerebrospinal fluid (CSF)) and nonbrain structures. Brain parenchymal fractions were calculated as the sum of GM and WM tissue volumes divided by total intracranial volume (GM + WM + CSF). GM images were used to create a study-specific template (using DARTEL, part of SPM), warped to the created template space, modulated (by multiplying each voxel's GM probability value by the Jacobian determinant derived from the nonlinear registration step in order to preserve the information regarding the amount of GM volume), registered to the Montreal Neurological Institute (MNI) standard space, and smoothed with an isotropic Gaussian kernel ($\sigma = 3$ mm).

Tract-based spatial statistics preprocessing

Diffusion-weighted images from Shariati imaging site and concatenated repetitions of diffusion-weighted images from Sina imaging site were corrected for the effects of motion and eddy current (using the *eddy_correct* function in the FMRIB's diffusion toolbox (FDT), part of FSL). Images from the Sina site were then split back to the original two and averaged in order to make a single diffusion-weighted image used in further analyses. After brain extraction, fractional anisotropy (FA) images were created by fitting a tensor model at each voxel to the diffusion data (using *dtifit* function in FDT). FA images were then preprocessed using tract-based spatial statistics (TBSS),²¹ part of FSL. Briefly, FA maps were nonlinearly registered to the MNI space and averaged to create a mean FA image. The resulting image was skeletonized, and individual FA skeleton maps were created by projecting the local FA maxima from each participant's aligned FA map onto the mean FA skeleton. In order to confine the analysis to WM, the FA skeleton threshold was then set to 0.2 (TBSS default).

Magnetization transfer ratio voxel-based analysis preprocessing

MT_{ON} and MT_{OFF} images were linearly registered to the corresponding T₁-weighted images (using FLIRT, part of FSL). Magnetization transfer ratio (MTR) images were calculated using the following formula

Tehran, Iran/Kimel Family Translational Imaging-Genetics Laboratory, Research Imaging Centre, Campbell Family Mental Health Research Institute, Centre for Addiction and Mental Health, Toronto, ON, Canada; Department of Psychiatry, University of Toronto, Toronto, ON, Canada; Mallinckrodt Institute of Radiology, Washington University School of Medicine, St. Louis, MO, USA

$$\text{MTR} = \frac{\text{MT}_{\text{OFF}} - \text{MT}_{\text{ON}}}{\text{MT}_{\text{OFF}}} \times 100$$

T_1 -weighted images were used to create a template (using *buildtemplateparallel.sh* script, part of Advanced Normalization Tools (ANTs) v1.9, <http://stnava.github.io/ANTs/>). MTR images were warped to the template space and masked with the WM masks from the brain tissue segmentation step. The masked MTR images and WM masks were both smoothed with an isotropic Gaussian kernel ($\sigma = 3$ mm). To compensate for the effects of spatial smoothing with surrounding zero voxels, the smoothed MTR images were divided by the smoothed WM masks.²²

Statistical analysis

All voxel-wise statistical analyses were performed nonparametrically using permutation-based approaches (10,000 permutations). Threshold-free cluster enhancement approach with family-wise error (FWE) correction was used to control for multiple comparisons across the voxels.²³ FWE-corrected $p < 0.05$ was considered significant. *Randomize* (part of FSL) was used to perform permutation tests assessing the additive effects of C3R102G genotype on WM MTR while accounting for the effects of age, sex, handedness, and disease duration. Given that T_1 -weighted and diffusion-weighted data were acquired using two different imaging protocols and scanners, a mega-analytic approach was used for TBSS and VBM to combine the Shariati and Sina datasets. Permutation-based mega-analysis was conducted using permutation analysis of linear models (PALM; <http://fsl.fmrib.ox.ac.uk/fsl/fslwiki/PALM>), where shuffling of data is only allowed within block (i.e. within data from each scan site).²⁴ Additive effects of C3R102G were modeled while adjusting for the effects of age, sex, handedness, disease duration, and scan site.

Statistical analyses on clinical, cognitive, and global imaging measures were conducted in the R environment (v3.0.2). General linear models were fitted to investigate the additive effects of C3R102G on clinical and cognitive outcomes, while adjusting for the fixed effects of age, sex, and disease duration. Linear mixed models were fitted using the *lmer* function (part of *lme4* and *lmerTest* packages in R) to investigate the additive effects of C3R102G genotype on brain parenchymal fraction and lesion load, while adjusting for the fixed effects of age, sex, and disease duration, and the random effects of scan site.

Results

Clinical severity, cognitive function, and global imaging measures

Data from 161 participants were used in this study. Demographic characteristics of the participants are summarized in Table 1. While C3R102G showed no significant effect on clinical severity (EDSS: $t = 0.17$, $p = 0.87$, $n = 152$; MSFC: $t = -1.27$, $p = 0.21$, $n = 146$) in our sample, higher C3-102G dosage was associated with worse cognitive performance ($t = -2.33$, $p = 0.02$, $n = 138$), greater brain atrophy as measured by lower brain parenchymal fraction ($t = -2.96$, $p = 0.0036$, $n = 155$), and greater lesion burden ($t = 2.24$, $p = 0.025$, $n = 154$). Post hoc analyses on the subcomponents of the composite cognitive score and MSFC revealed significant associations with PASAT ($t = -2.22$, $p = 0.03$) and SDMT ($t = -2.35$, $p = 0.02$). However, the results for 25FWT ($t = -0.15$, $p = 0.87$) and 9HPT ($t = -0.47$, $p = 0.63$) were nonsignificant. Although the association with CVLT was not significant ($t = -1.62$, $p = 0.11$), the direction of effect was consistent with the other cognitive tests. Adjusting for treatment status did not affect the results (EDSS: $p = 0.76$, MSFC: $p = 0.18$, composite cognitive score: $p = 0.02$, brain parenchymal fraction: $p = 0.004$, and lesion load: $p = 0.026$).

Regional GM atrophy

T_1 -weighted images from 155 participants were available for VBM (Sina: $n = 90$, Shariati: $n = 65$). VBM demonstrated that higher C3-102G dosage was associated with lower regional GM volume in left rostral hippocampus and amygdala (peak FWE-corrected $p = 0.014$, $X = -19$, $Y = -11$, $Z = -18$; size = 3688 mm³), left insular cortex and putamen (peak FWE-corrected $p = 0.036$, $X = -36$, $Y = +3$, $Z = +3$; size = 2850 mm³), right posterior thalamus and hippocampal tail (peak FWE-corrected $p = 0.037$, $X = +12$, $Y = -36$, $Z = +6$; size = 1248 mm³), left caudate nucleus (peak FWE-corrected $p = 0.043$, $X = -12$, $Y = +21$, $Z = -3$; size = 1092 mm³), and left posterior thalamus (peak FWE-corrected $p = 0.047$, $X = -10$, $Y = -30$, $Z = -8$; size = 93 mm³; Figure 1(a)). There was a similar trend (FWE-corrected $p < 0.10$) in right and left accumbens nuclei, middle temporal gyri, anterior parts of both thalamic nuclei, right caudate, amygdala, hippocampus, and frontal pole. Post hoc analysis on mean GM measure from the significant region of interest showed that the results were not confounded by treatment status (unadjusted and adjusted p for treatment status = 6.3×10^{-6} and 1.7×10^{-5} , respectively) and revealed

Table 1. Participant characteristics.

	Whole sample (<i>n</i> = 161)	rs2230199*	
		GG (<i>n</i> = 101)	GC/CC (<i>n</i> = 60)
(a) Demographics			
Age (years; mean ± SD)	31.8 ± 8.1	31.4 ± 8.3	32.5 ± 7.8
Sex (% female)	78%	79%	77%
Disease duration (years; mean ± SD)	7.0 ± 4.7	7.0 ± 4.6	7.0 ± 5.1
Disease modifying treatment (% treated)§	124 (77%)	78 (77%)	46 (77%)
Handedness (% right)	91%	88%	92%
(b) Available MRI data			
T1-weighted MRI (Sina/Shariati)	155 (90/65)	96 (56/40)	59 (34/25)
Diffusion tensor imaging (Sina/Shariati)	105 (48/57)	69 (34/35)	36 (14/22)
Magnetization transfer imaging (Sina)	90	56	34
(c) Clinical, cognitive, and global imaging measures			
EDSS score (mean ± SD)	2.75 ± 1.45	2.73 ± 1.45	2.80 ± 1.46
MSFC score (mean ± SD)	0.03 ± 0.72	0.08 ± 0.69	-0.07 ± 0.76
Cognitive <i>z</i> -score¶ (mean ± SD)	0.001 ± 0.84	0.12 ± 0.81	-0.19 ± 0.86
PASAT score¶	43.3 ± 11.3	44.9 ± 11.1	41.1 ± 11.3
SDMT score¶	49.0 ± 15.8	51.6 ± 16.0	45.8 ± 15.2
CVLT total learning score	54.5 ± 9.8	55.5 ± 9.7	52.5 ± 10.1
Brain parenchymal fraction¶ (%; mean ± SD)	80.68 ± 3.40	81.25 ± 2.99	79.76 ± 3.84
Lesion load¶ (cm ³ ; mean ± SD)	10.95 ± 9.49	9.91 ± 8.82	12.63 ± 10.33
*Given the low number of CC homozygotes, CC (<i>n</i> = 6) and GC (<i>n</i> = 54) carriers are grouped together for the convenience of comparison. rs2230199 minor allele frequency = 21%.			
§All patients were receiving either beta-interferon or no disease-modifying treatment, except for one receiving natalizumab and one receiving glatiramer acetate who were excluded from the analyses that included disease-modifying treatment as a covariate.			
¶ <i>p</i> < 0.05 in association with the additive effects of rs2230199, while adjusting for the effects of age, sex, disease duration, and imaging site (if applicable).			

significant effects on regional GM atrophy in both imaging sites (Sina: $p = 0.00007$, Shariati: $p = 0.03$), suggesting that the findings were not site specific (Figure 1(b)).

Regional WM demyelination and microstructural integrity

TBSS was performed on data from 105 participants (Sina: $n = 48$; Shariati: $n = 57$). Significantly lower FA was observed with higher number of C3-102G alleles in the body and genu of corpus callosum, left and right posterior thalamic radiations, anterior and superior corona radiata, cingulum bundles, and short association fibers (peak FWE-corrected $p = 0.0097$, $X = +17$, $Y = -13$, $Z = +35$, size = 15,121 mm³; Figure 2(a)). Post hoc analysis on mean FA of the significant regions demonstrated similar effects in data from both imaging sites (Sina: $p = 0.0006$, Shariati: $p = 0.003$; Figure 2(b)).

MTR voxel-based analysis (Sina: $n = 90$) revealed significantly lower MTR associated with higher

number of C3-102G alleles in the WM adjacent to the body, temporal horn, and posterior horn of the right lateral ventricle (peak FWE-corrected $p = 0.024$, $X = +27$, $Y = -56$, $Z = +17$, size = 13,360 mm³), anterior horn of the right lateral ventricle (peak FWE-corrected $p = 0.034$, $X = +27$, $Y = +24$, $Z = +19$, size = 4940 mm³), and in the right superior corona radiata (peak FWE-corrected $p = 0.045$, $X = +25$, $Y = -2$, $Z = +32$, size = 1657 mm³; Figure 3). A similar trend was observed around the posterior horn of the left lateral ventricle (FWE-corrected $p = 0.14$). Adjusting for treatment status did not affect the results from the significant regions (mean FA: unadjusted and adjusted $p = 1.6 \times 10^{-5}$ and 9.2×10^{-5} , respectively; mean MTR: unadjusted and adjusted $p = 1.7 \times 10^{-4}$ and 6.5×10^{-4} , respectively).

Discussion

We found convergent evidence from multiple imaging modalities that carrying higher copy numbers of C3-102G (which is linked to enhanced alternative

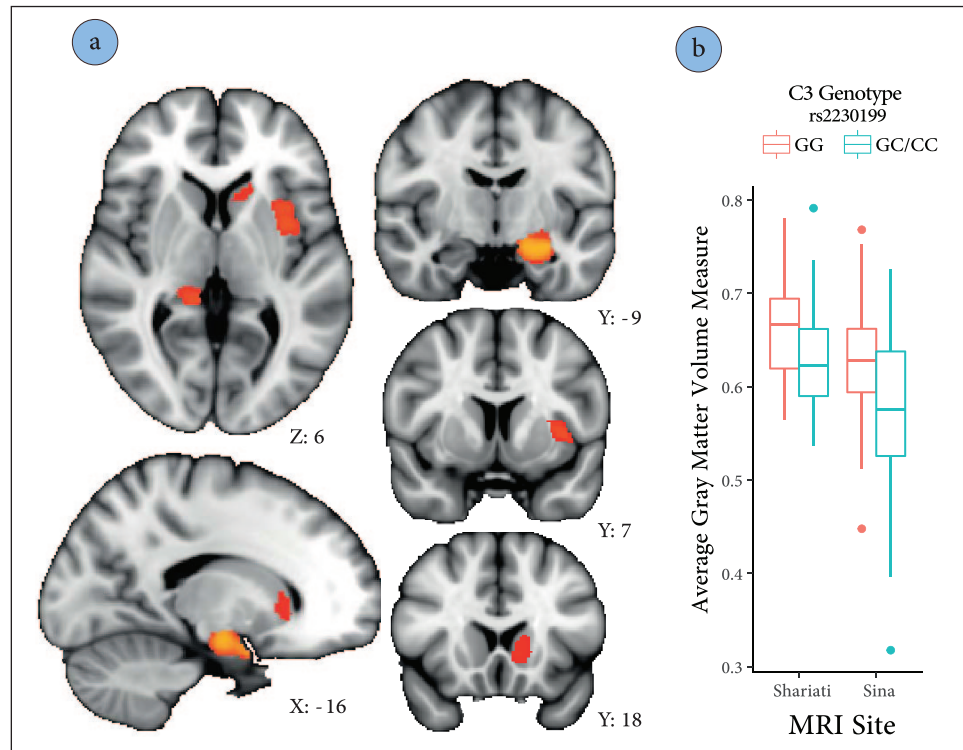


Figure 1. (a) Additive effect of C3R102G on regional gray matter atrophy in MS patients controlled for the effects of age, sex, disease duration, and imaging site. Clusters with significantly reduced gray matter volume are shown in colors (thresholded at family-wise error–corrected $p < 0.05$). (b) The effect of C3R102G on average mean gray matter volume from the significant region of interest depicted in (a) for each imaging site.

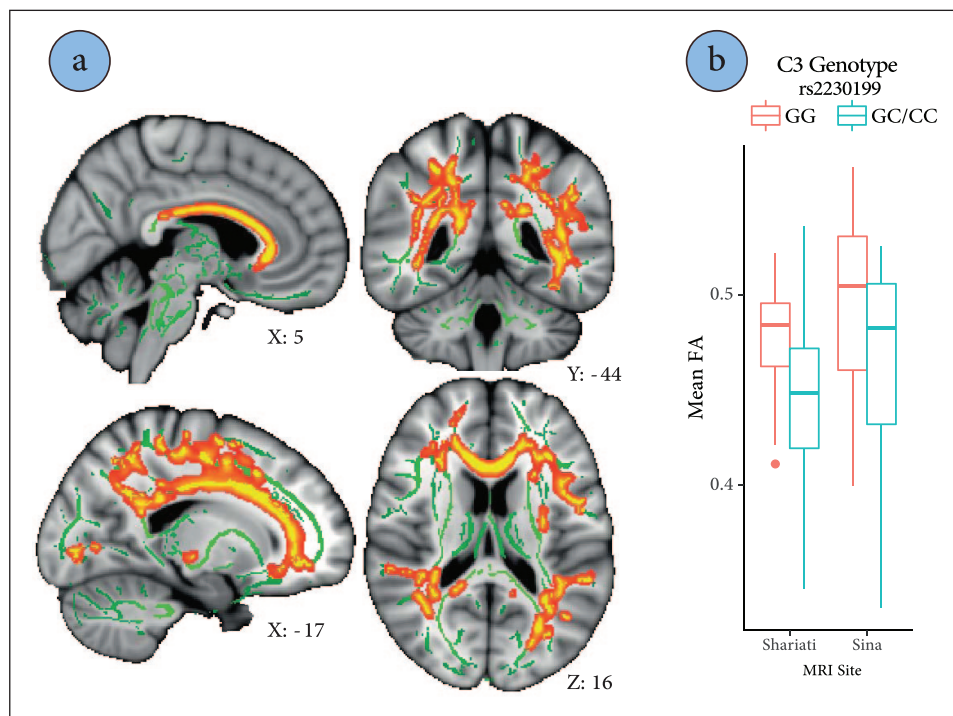


Figure 2. (a) Additive effect of C3R102G on white matter tracts fractional anisotropy skeleton in MS patients controlled for the effects of age, sex, disease duration, and imaging site. Clusters with significantly reduced fractional anisotropy are shown in yellow (thresholded at family-wise error–corrected $p < 0.05$). Mean skeleton is demonstrated in green. (b) The effect of C3R102G on average fractional anisotropy of the significant voxels depicted in (a) for each imaging site.

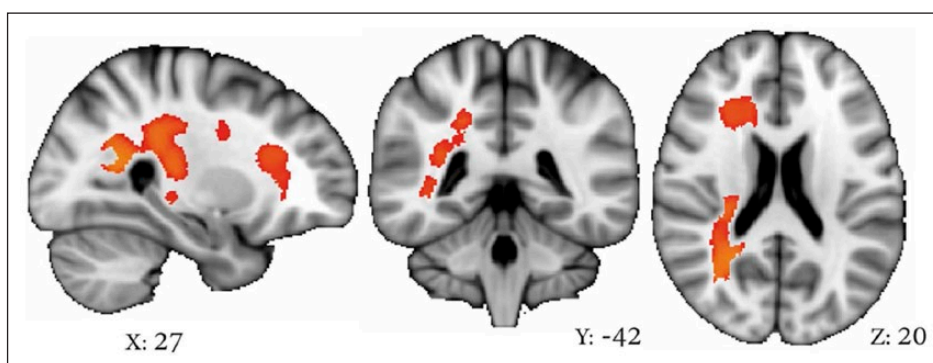


Figure 3. Additive effect of C3R102G on regional white matter magnetization transfer ratio in MS patients controlled for the effects of age, sex, and disease duration. Clusters with significantly reduced magnetization transfer ratio are shown in colors (thresholded at family-wise error-corrected $p < 0.05$).

complement pathway activity and higher C3 capacity to bind mononuclear cells) is associated with worse neuroimaging outcomes in individuals with MS. C3-102G was associated with lower brain parenchymal fraction, greater regional GM atrophy, higher WM lesion load, greater regional WM demyelination, and widespread loss of WM tract microstructural integrity. Although no significant effect was observed in our sample on the physical disability of MS patients, C3-102G was associated with poorer cognitive performance, particularly processing speed.

C3-102G was significantly associated with greater demyelination (as indexed by lower MTR) predominantly in the periventricular area. The predominantly periventricular areas affected by C3 genotype may support the possibility of ventricular CSF as the source for C3, which leaks through ependymal layer and is eventually deposited in the WM.² C3-102G showed a more diffuse effect on WM tract integrity. This may be explained by differences in sample size ($n = 90$ for MTR vs $n = 105$ for tracts FA) and image analysis approaches (skeleton-based TBSS for FA vs voxel-based analysis for MTR).

We also showed that C3-102G variation affects brain atrophy both globally and locally (primarily in subcortical areas such as amygdala, striatum, thalamus, and hippocampus) in MS patients. Of note, C3-102G (or its proxy SNP: rs11569415, $r^2 = 0.98$) is not associated with the volumes of subcortical structures in the enhancing neuroimaging genetics through meta-analysis (ENIGMA) genome-wide association studies (all p -values > 0.2),^{25,26} which suggests that the observed effects are specific to MS rather than healthy controls. Our results are in line with the findings from a recent study focused on hippocampus pathology in MS demonstrating C3 activation products localized at microglia-engulfed synapses.⁷

However, our findings on the effect of C3-102G on global and regional GM atrophy suggest that this pathology may not be limited to hippocampus in MS. Complement system and C3 activation has previously been shown to mediate phagocytosis of synapses and synaptic pruning during development,^{27,28} normal ageing,²⁹ and CNS neurodegenerative conditions such as frontotemporal dementia³⁰ and Alzheimer's disease.³¹ Although synaptic loss can be considered as the mechanism underlying the observed C3-related GM atrophy in MS, various other reasons including neuronal loss and demyelination may also result in GM atrophy.^{32,33}

Regardless of the modality, C3-102G was consistently associated with a worse outcome. This variant results in a conformational change in the structure of C3 (also in C3b and C3d),³⁴ which makes C3 a more potent activator of the alternative pathway, resistant to inhibition by major complement regulators, and results in a greater binding capacity of C3 to mononuclear cells.^{11,12} In line with our findings, experimental autoimmune encephalomyelitis (EAE; the animal model of MS) mice with double knockout of C3 gene ($C3^{-/-}$) showed less macrophage and T-cell infiltration in CNS, no microglial priming, markedly lower demyelination, and reduced disease severity compared with the control group,³⁵ while a mouse strain lacking the major regulator of the complement system in rodents, which is normally expressed by microglia, has demonstrated increased microglial priming and accelerated and exacerbated EAE.¹¹ In humans, higher CSF C3 levels have been linked to progressive MS, higher CSF neurofilament light concentration (a marker of neurodegeneration), MRI lesion burden, and disease severity.³⁶ Taken together, these findings suggest that higher C3 activity may result in greater disease progression and severity in MS.

Although C3-102G was associated with greater brain tissue damage as evident in MRI (both GM atrophy and WM demyelination) and worse cognitive performance, its effect was not significant on the severity of physical disability. This may be due to the relatively small sample size of this study to detect effects on less sensitive scales such as EDSS. Although not to the same extent as C3, other components of complement system such as C1q, complement regulators (e.g. factor H), and downstream complement components have also been reported in MS pathology and/or implicated in the progression of the disease.^{5,37} Functional variants in some of these complement components have also been identified.¹¹ Nevertheless, in this study, we focused only on C3 due to its central role in complement activation and the wealth of evidence supporting its involvement in MS pathophysiology. Future studies with much larger sample size may be able to combine genetic variants in different components of the complement system and assess potential interplays among these polymorphisms on MS severity. Finally, employing other imaging modalities that are sensitive to GM demyelination (e.g. high-resolution MTR or relaxometry), neuroinflammation (e.g. positron emission tomography³⁸), or retinal degeneration using optical coherence tomography may further our understanding of the effects of complement system activation in MS.

In conclusion, our study provides support for potential causal role of the complement system (especially C3) in the pathophysiology of MS and introduces a functional C3 genetic variant as a source of heterogeneity in disease severity in MS patients.

Acknowledgements

T.R., S.S., and A.N. were recipients of the Jacqueline Du Pré grant, Multiple Sclerosis International Federation.


Declaration of Conflicting Interests

The author(s) declared no potential conflicts of interest with respect to the research, authorship, and/or publication of this article.

Funding

The author(s) disclosed receipt of the following financial support for the research, authorship, and/or publication of this article: T.R. was funded by the Isabel Johnson Biomedical Postdoctoral Award, Alzheimer Society of Canada Research Program. A.N. was supported by the Canadian Institutes of Health Research Fellowship Award. Data gathering for the study was supported by grants from Tehran University of Medical Sciences and MS Society of Iran. The funding sources had no influence on the writing of this manuscript or the decision to submit it for publication.

ORCID iD

Arash Nazeri  <https://orcid.org/0000-0001-6983-0641>

References

1. Sospedra M and Martin R. Immunology of multiple sclerosis. *Annu Rev Immunol* 2005; 23: 683–747.
2. Adams CW, Abdulla YH, Torres EM, et al. Periventricular lesions in multiple sclerosis: Their perivenous origin and relationship to granular ependymitis. *Neuropathol Appl Neurobiol* 1987; 13: 141–152.
3. Brink BP, Veerhuis R, Breij EC, et al. The pathology of multiple sclerosis is location-dependent: No significant complement activation is detected in purely cortical lesions. *J Neuropathol Exp Neurol* 2005; 64: 147–155.
4. Barnett MH, Parratt JD, Cho ES, et al. Immunoglobulins and complement in postmortem multiple sclerosis tissue. *Ann Neurol* 2009; 65: 32–46.
5. Ingram G, Loveless S, Howell OW, et al. Complement activation in multiple sclerosis plaques: An immunohistochemical analysis. *Acta Neuropathol Commun* 2014; 2: 53.
6. Prineas JW, Kwon EE, Cho ES, et al. Immunopathology of secondary-progressive multiple sclerosis. *Ann Neurol* 2001; 50: 646–657.
7. Michailidou I, Willems JG, Kooi EJ, et al. Complement C1q-C3-associated synaptic changes in multiple sclerosis hippocampus. *Ann Neurol* 2015; 77: 1007–1026.
8. Ramaglia V, Hughes TR, Donev RM, et al. C3-dependent mechanism of microglial priming relevant to multiple sclerosis. *Proc Natl Acad Sci USA* 2012; 109: 965–970.
9. Perry VH and Holmes C. Microglial priming in neurodegenerative disease. *Nat Rev Neurol* 2014; 10: 217–224.
10. Priya RR, Chew EY and Swaroop A. Genetic studies of age-related macular degeneration: Lessons, challenges, and opportunities for disease management. *Ophthalmology* 2012; 119: 2526–2536.
11. Heurich M, Martínez-Barricarte R, Francis NJ, et al. Common polymorphisms in C3, factor B, and factor H collaborate to determine systemic complement activity and disease risk. *Proc Natl Acad Sci USA* 2011; 108: 8761–8766.
12. Arvilommi H. Capacity of complement c3 phenotypes to bind on to mononuclear cells in man. *Nature* 1974; 251: 740–741.

13. Enzinger C, Barkhof F, Ciccarelli O, et al. Nonconventional MRI and microstructural cerebral changes in multiple sclerosis. *Nat Rev Neurol* 2015; 11: 676–686.
14. Roostaei T, Sadaghiani S, Park MT, et al. Channelopathy-related SCN10A gene variants predict cerebellar dysfunction in multiple sclerosis. *Neurology* 2016; 86: 410–417.
15. Kurtzke JF. Rating neurologic impairment in multiple sclerosis: An expanded disability status scale (EDSS). *Neurology* 1983; 33: 1444–1452.
16. Eshaghi A, Riyahi-Alam S, Roostaei T, et al. Validity and reliability of a Persian translation of the minimal assessment of cognitive function in multiple sclerosis (MACFIMS). *Clin Neuropsychol* 2012; 26: 975–984.
17. Parmenter BA, Weinstock-Guttman B, Garg N, et al. Screening for cognitive impairment in multiple sclerosis using the symbol digit modalities test. *Mult Scler* 2007; 13: 52–57.
18. Bazyar N, Azarpira N, Khatami SR, et al. The investigation of allele and genotype frequencies of human C3 (rs2230199) in south Iranian population. *Mol Biol Rep* 2012; 39: 8919–8924.
19. Sahraian A and Radü EW. *MRI atlas of MS lesions*. Berlin: Springer, 2007.
20. Ashburner J and Friston KJ. Voxel-based morphometry—the methods. *Neuroimage* 2000; 11: 805–821.
21. Smith SM, Jenkinson M, Johansen-Berg H, et al. Tract-based spatial statistics: Voxelwise analysis of multi-subject diffusion data. *Neuroimage* 2006; 31: 1487–1505.
22. Lee JE, Chung MK, Lazar M, et al. A study of diffusion tensor imaging by tissue-specific, smoothing-compensated voxel-based analysis. *Neuroimage* 2009; 44: 870–883.
23. Smith SM and Nichols TE. Threshold-free cluster enhancement: Addressing problems of smoothing, threshold dependence and localisation in cluster inference. *Neuroimage* 2009; 44: 83–98.
24. Winkler AM, Webster MA, Vidaurre D, et al. Multi-level block permutation. *Neuroimage* 2015; 123: 253–268.
25. Hibar DP, Stein JL, Renteria ME, et al. Common genetic variants influence human subcortical brain structures. *Nature* 2015; 520: 224–229.
26. Hibar DP, Adams HH, Jahanshad N, et al. Novel genetic loci associated with hippocampal volume. *Nat Commun* 2017; 8: 13624.
27. Stevens B, Allen NJ, Vazquez LE, et al. The classical complement cascade mediates CNS synapse elimination. *Cell* 2007; 131: 1164–1178.
28. Schafer DP, Lehrman EK, Kautzman AG, et al. Microglia sculpt postnatal neural circuits in an activity and complement-dependent manner. *Neuron* 2012; 74: 691–705.
29. Shi Q, Colodner KJ, Matousek SB, et al. Complement C3-deficient mice fail to display age-related hippocampal decline. *J Neurosci* 2015; 35: 13029–13042.
30. Lui H, Zhang J, Makinson SR, et al. Progranulin deficiency promotes circuit-specific synaptic pruning by microglia via complement activation. *Cell* 2016; 165: 921–935.
31. Chung WS, Verghese PB, Chakraborty C, et al. Novel allele-dependent role for APOE in controlling the rate of synapse pruning by astrocytes. *Proc Natl Acad Sci USA* 2016; 113: 10186–10191.
32. Vercellino M, Masera S, Lorenzatti M, et al. Demyelination, inflammation, and neurodegeneration in multiple sclerosis deep gray matter. *J Neuropathol Exp Neurol* 2009; 68: 489–502.
33. Papadopoulos D, Dukes S, Patel R, et al. Substantial archaeocortical atrophy and neuronal loss in multiple sclerosis. *Brain Pathol* 2009; 19: 238–253.
34. Rodriguez E, Nan R, Li K, et al. A revised mechanism for the activation of complement C3 to C3b: A molecular explanation of a disease-associated polymorphism. *J Biol Chem* 2015; 290: 2334–2350.
35. Nataf S, Carroll SL, Wetsel RA, et al. Attenuation of experimental autoimmune demyelination in complement-deficient mice. *J Immunol* 2000; 165: 5867–5873.
36. Aeinehband S, Lindblom RP, Al Nimer F, et al. Complement component C3 and butyrylcholinesterase activity are associated with neurodegeneration and clinical disability in multiple sclerosis. *PLoS ONE* 2015; 10: e0122048.
37. Ingram G, Hakobyan S, Hirst CL, et al. Complement regulator factor H as a serum biomarker of multiple sclerosis disease state. *Brain* 2010; 133: 1602–1611.
38. Hagens M, van Berckel B and Barkhof F. Novel MRI and PET markers of neuroinflammation in multiple sclerosis. *Curr Opin Neurol* 2016; 29: 229–236.